

## Foldameric $\alpha/\beta$ -Peptide Analogs of the $\beta$ -Sheet-Forming Antiangiogenic Anginex: Structure and Bioactivity

Zsófia Hegedüs,<sup>†,§</sup> Edit Wéber,<sup>†,§</sup> Éva Kriston-Pál,<sup>‡</sup> Ildikó Makra,<sup>‡</sup> Ágnes Czibula,<sup>‡</sup> Éva Monostori,<sup>‡</sup> and Tamás A. Martinek<sup>\*,†</sup>

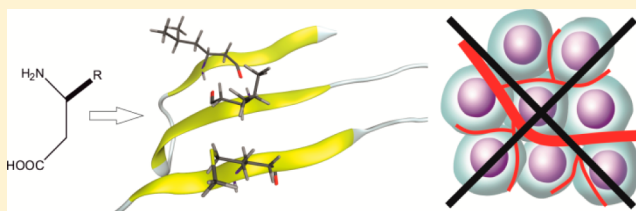
<sup>†</sup>SZTE-MTA Lendulet Foldamer Research Group, Institute of Pharmaceutical Chemistry, University of Szeged, Eötvös u. 6, H-6720 Szeged, Hungary

<sup>‡</sup>Lymphocyte Signal Transduction Laboratory, Institute of Genetics, Biological Research Center of the Hungarian Academy of Sciences, Temesvári krt. 62, H-6726 Szeged, Hungary

### S Supporting Information

**ABSTRACT:** The principles of  $\beta$ -sheet folding and design for  $\alpha$ -peptidic sequences are well established, while those for sheet mimetics containing homologated amino acid building blocks are still under investigation. To reveal the structure–function relations of  $\beta$ -amino-acid-containing foldamers, we followed a top-down approach to study a series of  $\alpha/\beta$ -peptidic analogs of anginex, a  $\beta$ -sheet-forming antiangiogenic peptide. Eight anginex analogs were developed by systematic  $\alpha \rightarrow \beta^3$

substitutions and analyzed by using NMR and CD spectroscopy. The foldamers retained the  $\beta$ -sheet tendency, though with a decreased folding propensity.  $\beta$ -Sheet formation could be induced by a micellar environment, similarly to that of the parent peptide. The destructuring effect was higher when the  $\alpha \rightarrow \beta^3$  exchange was located in the  $\beta$ -sheet core. Analysis of the  $\beta$ -sheet stability versus substitution pattern and the local conformational bias of the bulky  $\beta^3$ V and  $\beta^3$ I residues revealed that a mismatch between the H-bonding preferences of the  $\alpha$ - and  $\beta$ -residues played a minor role in the structure-breaking effect. Temperature-dependent CD and NMR measurements showed that the hydrophobic stabilization was scaled-down for the  $\alpha/\beta$ -peptides. Analysis of the biological activity of the foldamer peptides showed that four anginex derivatives dose-dependently inhibited the proliferation of a mouse endothelial cell line. The  $\alpha \rightarrow \beta^3$  substitution strategy applied in this work can be a useful approach to the construction of bioactive  $\beta$ -sheet mimetics with a reduced aggregation tendency and improved pharmacokinetic properties.



## INTRODUCTION

The design of water-soluble  $\beta$ -sheet models mimicking structural and functional features of proteins is an enduring challenge. The underlying principles of  $\beta$ -sheet folding and design for natural  $\alpha$ -peptidic sequences have been thoroughly studied.<sup>1–7</sup> *De novo* designed structures have been reported to form  $\beta$ -hairpins,<sup>8,9</sup> three-stranded  $\beta$ -sheets<sup>10–16</sup> and  $\beta$ -sandwiches.<sup>17–19</sup> Hairpins proved to be useful protein epitope mimetics with bioactive potencies.<sup>20</sup>

Foldameric sequences with unnatural building blocks in the chain are an important class of  $\beta$ -sheet mimetics. In a bottom-up approach, it has been shown that homologated amino acids can be utilized to build short turns<sup>21–25</sup> and cyclic  $\alpha/\beta$ -peptides as hairpin models.<sup>26</sup> Nonpeptidic template and turn units have been combined with peptides to construct parallel and antiparallel sheet structures, some of them having intriguing bioactivity.<sup>27,28</sup> Sheet-like self-organization has been found for  $\alpha/\beta$ -peptides at the air/water interface<sup>29</sup> and in fibrillous  $\beta$ -peptidic nanostructures.<sup>30–34</sup>

The top-down approach starting from  $\alpha$ -peptidic  $\beta$ -hairpins has revealed complex behavior when the  $\beta$ -amino acid substitutions are made in the hydrophobic core. In matching positions of the two strands, the  $\alpha \rightarrow \beta^3$  modification results in a changed H-bond pattern and an altered side-chain display as

compared with the natural  $\beta$ -sheet structure,<sup>35</sup> which leads to decreased structural stability. The alternative design strategies maintaining the native side-chain orientation substitute two  $\alpha$ -amino acid residues by a single  $\beta$ -amino acid ( $\alpha\alpha \rightarrow \beta^2$  or  $\beta^3$ ), or applies special  $\beta^{2,3}$ -residues.<sup>36</sup> These substitution strategies have been tested for 16-residue disulfide-cyclized  $\beta$ -hairpin peptides with a hydrophobic cluster of four amino acids. The focus has been placed on the structural stability, but these sequence changes may lead to the loss of key side-chains in a biologically active  $\beta$ -sheet. A 19mer hydrophobic sequence with  $\beta$ -amino acid substitutions was recently shown to form a three-stranded sheet structure in organic solvents.<sup>37</sup>

Whereas the top-down approach to construct bioactive foldameric helices has become successful,<sup>38</sup> the rules of possible  $\beta$ -amino acid replacements in a multiple-stranded water-soluble bioactive  $\beta$ -sheet still remain to be investigated. It is not known whether the core  $\alpha \rightarrow \beta$  mutations in a hydrophobically stabilized system cause the same alterations as in the hairpin models. Whether an  $\alpha \rightarrow \beta$  substituted  $\beta$ -sheet region can retain its biological activity is a particularly important question.

Received: August 4, 2013

Published: October 2, 2013

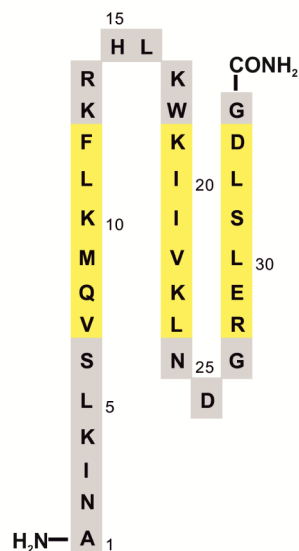
Our aim was a systematic probing of the effects of  $\beta^3$ -amino acid substitutions in a water-soluble, biologically active  $\beta$ -sheet-forming peptide. The 33mer peptide anginex, a designed  $\beta$ -sheet-forming peptide with antiangiogenic and antitumor activities,<sup>39–43</sup> was chosen as model system. Anginex forms a  $\beta$ -sandwich structure via association to dimers and tetramers at higher concentrations,<sup>10,44</sup> and upon interaction with *n*-dodecylphosphocholine (DPC) micelles.<sup>45</sup> In the concentration range of *in vitro* studies, its prevailing conformation is random coil,<sup>10,46</sup> but the three-stranded  $\beta$ -sheet-forming propensity is crucial for the antiangiogenic activity.<sup>46</sup> We hypothesize that the effects of the core  $\alpha \rightarrow \beta$  substitutions can be well detected in this relatively sensitive system, and the corresponding biological properties may be good indicators of the structural changes. We demonstrate here that the analogs with  $\alpha \rightarrow \beta^3$  substitutions in particular positions retain the inducible  $\beta$ -sheet-folding propensity of anginex. More importantly, they also exhibit biological activity compared to the maternal molecule indicating a close structure–function relationship.

## RESULTS

**Backbone Substitution Strategy.** The majority of residues in the sheet-forming region of anginex are crucial for bioactivity in *in vitro* tests.<sup>47,48</sup> These involve the side-chains responsible for the hydrophobic stabilization of the structure and interaction anchor points over the surface of anginex. To retain the side-chain chemistry,  $\beta^3$ -amino acids were chosen for the  $\alpha \rightarrow \beta$  substitutions. Avoiding sheet stabilization strategies with amino acid deletion<sup>36</sup> allowed us to monitor the structural adaptation of the system without losing bioactivity due to missing potential pharmacophore points. The  $\beta^3$ -residues may alter the peptide bond and side-chain orientations, and replacements in matching positions are therefore expected to minimize the destructuring effects. Triplets of  $\alpha$ -residues in matching positions were replaced along the three-stranded  $\beta$ -sheet (Figure 1). Six sequences (1–6) were designed with the in-registry substitution pattern covering the sheet-forming region over the distance of six residues. The length of the sheet segment enabled us to analyze the effects of the distance from the turn regions. Two additional sequences were constructed with nonmatching backbone homologations to test the hypothesis of matching replacements in this system: a diagonal (7), and a sequential pattern (8). These sequences allowed the investigation of several triplet substitutions, including various types of amino acids, as regards hydrophobicity, charge, side-chain volume and branching.

**Overall Folding Propensity.** As stated above, the  $\beta$ -sheet of anginex is highly sensitive to the conditions. NMR structure elucidation studies have revealed that a micelle-forming detergent, *n*-dodecylphosphocholine (DPC), induces its folding.<sup>45</sup> The CD analysis was therefore carried out in K-phosphate buffer at pH 5.6 with and without 2.5 mM DPC. The concentration of DPC was chosen to keep the background absorbance low, but above its critical micelle concentration,<sup>49–51</sup> to ensure micelle formation.

In buffer only, the CD curve of anginex with a minimum at around 217 nm proved the  $\beta$ -sheet structure of the 33mer (Figure 2A). The CD traces of the analogs shared a common minimum at around 200 nm, with variable intensity, and suggested partial folding. Small differences were observed in the shoulders near 217 nm, which were earlier used as indicator of  $\beta$ -sheet content for anginex-related  $\beta$ -sheet peptides.<sup>4</sup> Expressed relative to the CD intensity of anginex at 217 nm, the



anginex ANIKLSVQMKLFRHLKWKIIVKLNLDGRELSLDG-NH<sub>2</sub>

- 1 ANIKLS $\beta^3$ VQMKLFRHLKWKIIVK $\beta^3$ LNDG $\beta^3$ RELSLDG-NH<sub>2</sub>
- 2 ANIKLSV $\beta^3$ QMKLFRHLKWKIIV $\beta^3$ KLNDR $\beta^3$ ELSLDG-NH<sub>2</sub>
- 3 ANIKLSVQ $\beta^3$ MKLFKRHLKWKI $\beta^3$ VKLNDR $\beta^3$ LSLDG-NH<sub>2</sub>
- 4 ANIKLSVQMP $\beta^3$ KLFRHLKWKI $\beta^3$ VKLNDR $\beta^3$ SLDG-NH<sub>2</sub>
- 5 ANIKLSVQMK $\beta^3$ LFKRHLKWK $\beta^3$ IIVKLNDR $\beta^3$ LDG-NH<sub>2</sub>
- 6 ANIKLSVQMKL $\beta^3$ FRHLKWK $\beta^3$ KIIVKLNDR $\beta^3$ SLD-NH<sub>2</sub>
- 7 ANIKLSVQMK $\beta^3$ LFKRHLKWKI $\beta^3$ VKLNDR $\beta^3$ LSLDG-NH<sub>2</sub>
- 8 ANIKLSVQMKLFRHLKWK $\beta^3$ I $\beta^3$ VKLNDR $\beta^3$ SLDG-NH<sub>2</sub>

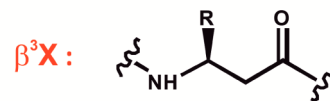


**Figure 1.** The three-stranded  $\beta$ -sheet alignment of anginex represented in one-letter code amino acid sequence, with the substitution patterns: in-registry (1–6), diagonal (7) and sequential (8) indicated with dotted lines. The yellow background indicates the sheet-forming regions of anginex. Side chains of  $\beta^3$ -amino acids are indicated by the standard  $\alpha$ -amino acid one-letter codes.

analog displayed  $\beta$ -sheet contents in the range 25–42% (Figure 2A, inset), which indicated their reduced folding propensities. Peptides 6 and 1, substituted at the edges of the  $\beta$ -sheet, exhibited the highest intensities.

The structuring effect of DPC on the analogs was clearly apparent in the CD curves (Figure 2B). The increased  $\beta$ -sheet content of anginex upon the addition of DPC was transparent only in the NMR spectra, whereas the CD profile displayed only minor changes. For 1–8, the minima shifted toward 210 nm, with a zero cross-point around 200 nm, and the intensity of the shoulders near 217 nm increased. DPC not only induced the formation of the  $\beta$ -sheet, but also enhanced the differences between the folding propensities of the analogs (Figure 2B, inset). The relative  $\beta$ -sheet content was in the range 61–98%, which suggested that an interacting partner can induce  $\beta$ -sheet formation. The destructuring effect of the  $\beta^3$ -amino acid insertions was position-dependent. The closer the  $\alpha \rightarrow \beta^3$  substitution was to the  $\beta$ -sheet core, the lower was the folding propensity. Sequences 7 and 8 did not show a significant difference from the in-registry mutated analogs (1–6),

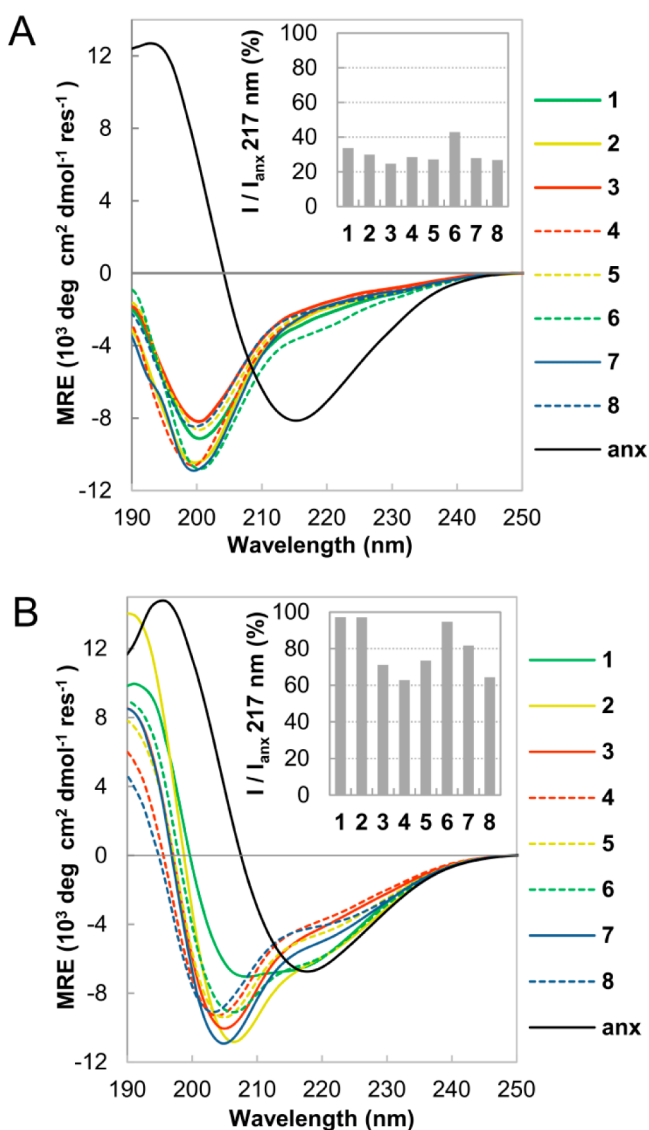


**Figure 2.** CD curves of anginex (anx) and its  $\alpha/\beta$ -analogs at 100  $\mu\text{M}$  and pH 5.6 without (A) and with (B) 2.5 mM DPC. Anginex/analog intensity ratios at 217 nm are displayed (inset).

indicating that there was no extra sheet-breaking effect due to the nonmatching local conformational behavior of the  $\beta$ - and the surrounding  $\alpha$ -residues.

**Conformation at the Residue-Level.** Chemical shift analysis<sup>52,53</sup> was used to gain a deeper insight into the  $\beta$ -sheet-forming propensity at the amino acid level. In the absence of DPC, heteronuclear NMR spectra were measured and assigned for the peptides in natural abundance under optimized concentration,<sup>10</sup> temperature and pH (Figure S1). All the identified NH, H $\alpha$ , C $\alpha$  and C $\beta$  resonances (Table S1) were included in the analysis. The secondary structure propensity (SSP) score<sup>54</sup> was calculated by using the ssp software. Resonances of the  $\beta^3$ -residues and glycines were excluded from the calculation, because of the lack of reference values and their poor  $\beta$ -sheet indicator property,<sup>54</sup> respectively. Although the secondary structure-independent neighborhood effect of the  $\beta^3$ -residues on the magnetic environment of the adjacent  $\alpha$ -residues can not be ruled out, we did not observe any major systematic influence on the secondary chemical shifts, such as outlier values around the  $\alpha \rightarrow \beta^3$  substitutions.

The SSP scores of anginex (Figures 3 and S2) in the second (K19–L24) and third (R28–D33) sheet segments were in the

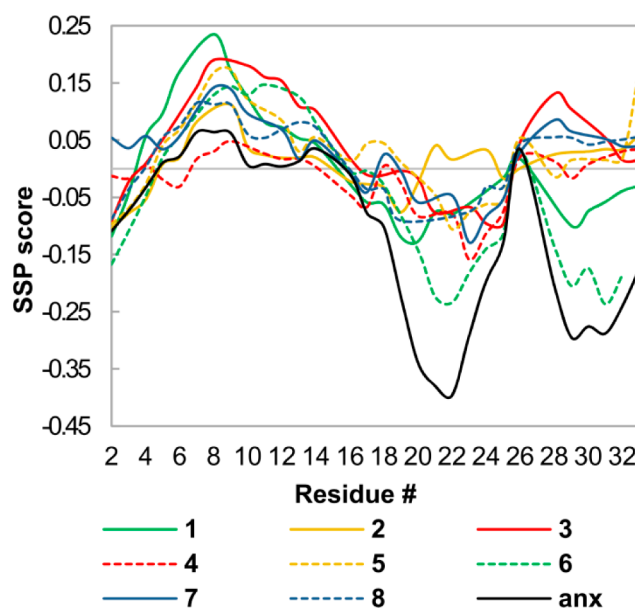


**Figure 3.** Envelopes of the SSP scores of anginex and its  $\alpha/\beta$ -analogs, derived from the chemical shifts measured in HEPES pH 5.6 at 500  $\mu\text{M}$ . For simplicity, the values next to the omitted residues are connected and the detailed results for the individual SSP scores for each residue are presented in Figure S2. The different NMR resonances for a given residue were combined into a single score between 1 and  $-1$ , providing a quantitative estimate of the fractional secondary structure. Positive and negative scores corresponded to helix and sheet structures, respectively. Because of the partial assignment, the N-terminal A1, N2 and the loop residue H15 were not included in the analysis.

range  $-0.18$  to  $-0.40$ , demonstrating the presence of the  $\beta$ -sheet conformation. The N-terminal part (V7–F12), however, exhibited SSP values corresponding to a random coil structure. This was in line with the earlier structural data for anginex, showing that the first strand of the  $\beta$ -sheet was more flexible than the other two.<sup>45</sup> Similar folding patterns were observed for the  $\alpha/\beta$ -analogs, but the overall sheet-forming tendencies of the second and third strands were lower than found for the parent anginex. The  $\beta^3$ -residues in the first strand induced low helical propensities, which was in line with the helix-promoting nature of these building blocks. The  $\beta$ -sheet content followed a similar trend as observed in CD experiments. Analogs with  $\alpha \rightarrow \beta^3$  mutations at the periphery of the  $\beta$ -sheet (1 and 6) displayed the highest overall  $\beta$ -sheet content. Substitutions in the core region shifted the SSP scores closer to the random coil values.

On addition of the structure-inducing DPC to the NMR samples, signal broadening was observed, which did not allow signal assignment and high-resolution structure analysis. We suppose that the origin of the resonance broadening was an intermediate time-scale chemical exchange between the  $\beta$ -sheet and the disordered populations.<sup>4</sup> Nevertheless, downfield-shifted signals of anginex appeared at around 5–6 and 8.5–9.5 ppm for the H $\alpha$  and NH resonances, respectively (Figures S3 and S4), which indicated a predominant  $\beta$ -sheet. For the  $\alpha/\beta$ -analogs, the most pronounced resonance broadening was observed for 1 and 6 (Figure S4). For 1, signals of H $\alpha$  protons could also be identified at around 5–5.5 ppm, and the

corresponding  $H\alpha$ – $H\alpha$  NOE peaks were also detected, demonstrating the increased  $\beta$ -sheet content (Figure S5).

The local conformational flexibility of the  $\beta^3$ -residues could be indicated by the chemical shift difference ( $\Delta\delta$ ) observed for the diastereotopic  $H\alpha$  protons. We found nonuniform behavior for the  $\Delta\delta$  values in the  $\beta$ -amino acids (Table S2). For the  $\beta^3V$ - and  $\beta^3I$ -residues, the  $\Delta\delta$  values were in the range 0.14–0.24 ppm, i.e., systematically higher than the average  $\Delta\delta$  (0.11 ppm), indicating increased local rigidity. It has been reported that side-chain branching adjacent to the  $\beta$ -carbon atom stabilizes the H14-helix,<sup>55</sup> which is possible only if there is a propensity to attainment of a gauche  $\theta$  torsion. To test whether the increased rigidity was a result of a gauche conformational bias, we analyzed the  $^3J(H\alpha-H\beta)$  couplings and the  $H\alpha$ –NH NOE intensity patterns around the  $\beta^3V$ - and  $\beta^3I$ -residues.

Large  $^3J(H\alpha1-H\beta)$  ( $>10$  Hz) values were uniformly accompanied by elevated  $I_{NOE}(H\alpha1-NH)/I_{NOE}(H\alpha2-NH)$  ratios, indicating a conformational bias toward the local conformation C (Figure 4). The gauche conformation C was

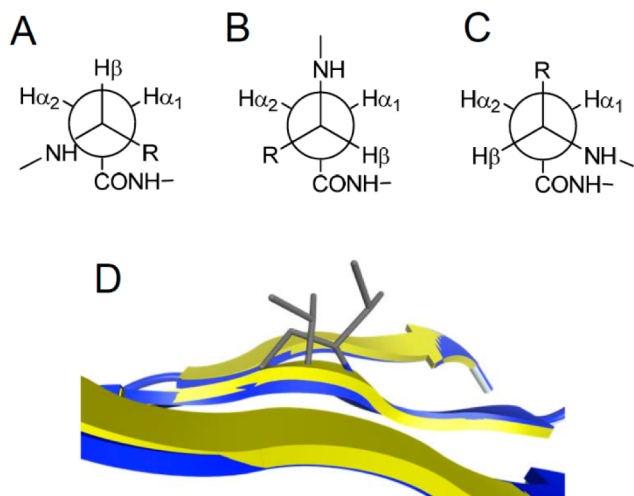


**Figure 4.** Schematic representation of the three local minima around the  $\theta$  torsion of the  $\beta^3$ -residues: gauche – (A), antiperiplanar (B), and gauche + (C). The combination of  $^3J(H\alpha1-H\beta) >10$  Hz and  $I_{NOE}(H\alpha1-NH)/I_{NOE}(H\alpha2-NH) > 1.5$  indicates a bias toward conformation C. Modeled local geometry of  $\beta^3V22$  (yellow backbone) within the  $\beta$ -sheet, and its comparison with the parent structure (blue backbone) (D). The modeling protocol is given in the Supporting Information text.

compatible with the geometrical requirements of a  $\beta$ -sheet in terms of accommodation to the H-bonding network. On the other hand, the side-chain orientation and the overall backbone curvature supported the hypothesis that these homologated residues did not properly fit into the closely packed hydrophobic cluster of surrounding  $\alpha$ -residues.

**Effects on the Hydrophobic Forces and Self-Association.** Hydrophobically driven oligomerization of anginex at elevated concentrations plays important roles in the stabilization of the  $\beta$ -sheet.<sup>44</sup> In order to test the presence of this phenomenon for the  $\alpha/\beta$ -derivatives, pulsed field-gradient spin echo (PFGSE) Diffusion Ordered Spectroscopy (DOSY) NMR measurements were carried out. With an apparent hydrodynamic radius of 15.6 Å, the positive control anginex formed tetramers at the concentration of 500  $\mu$ M at 37 °C (Table 1). This finding was in good agreement with the literature data.<sup>10,44</sup> From CD and independent NMR data, increased disorder was

**Table 1.** Estimated Diffusion Coefficients ( $D$ ) and Apparent Hydrodynamic Radii ( $r$ ) Derived from DOSY NMR Measurements

	$D$ ( $10^{-10}$ m <sup>2</sup> s <sup>-1</sup> )	$r$ (Å)
anx	2.11	15.6
1	2.20	14.9
2	2.25	14.6
3	2.27	14.5
4	2.23	14.8
5	2.27	14.5
6	2.35	14.0
7	2.25	14.6
8	2.29	14.4

observed for the foldameric analogs, which has a radius increasing effect for a single chain without oligomerization.<sup>56</sup> The analogs (1–8) exhibited apparent hydrodynamic radii in the range 14.0–14.9 Å indicating a small decrease relative to anginex. This can be explained by a diminished tendency to self-association for  $\alpha/\beta$ -derivatives, which counteracts the increased dimensions of the partially unfolded chains.

Besides the aggregation phenomena, hydrophobic forces also facilitate the intrachain clustering of the hydrophobic side chains, thereby stabilizing the  $\beta$ -sheet fold. The hydrophobic stabilization effect scales up with temperature,<sup>57</sup> which allows testing of the presence and the weight of these interactions. Temperature-dependent CD curves were analyzed, and higher CD intensities (at 217 nm) were observed for anginex and its analogs (1–8) at elevated temperatures (Figures 5 and S6). For

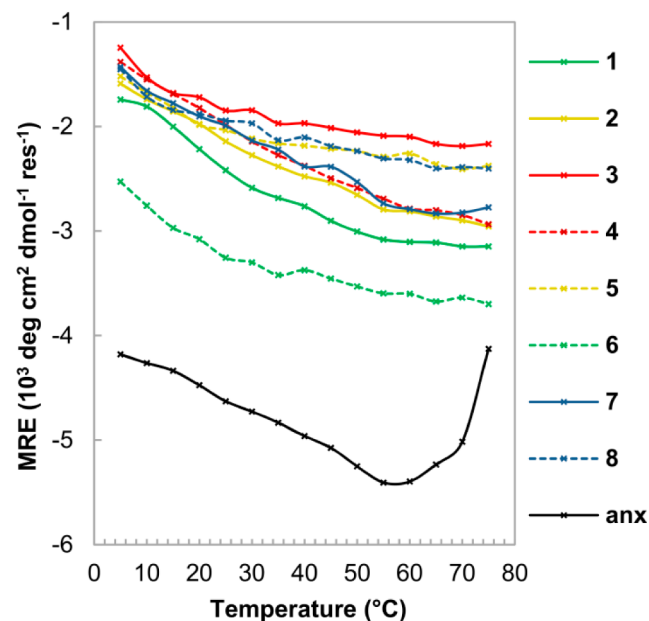


**Figure 5.** Mean residue ellipticity values at 217 nm versus temperature in the range 5–75 °C.

anginex, the maximum CD intensity was at around 55 °C, and the ellipticity decreased at higher temperatures (structural melt). The analogs exhibited a monotonous enhancement in  $\beta$ -sheet content from 5 to 75 °C, though with lower overall negative slopes, pointing to a lower hydrophobic contribution. Further, the negative temperature gradient was highest for

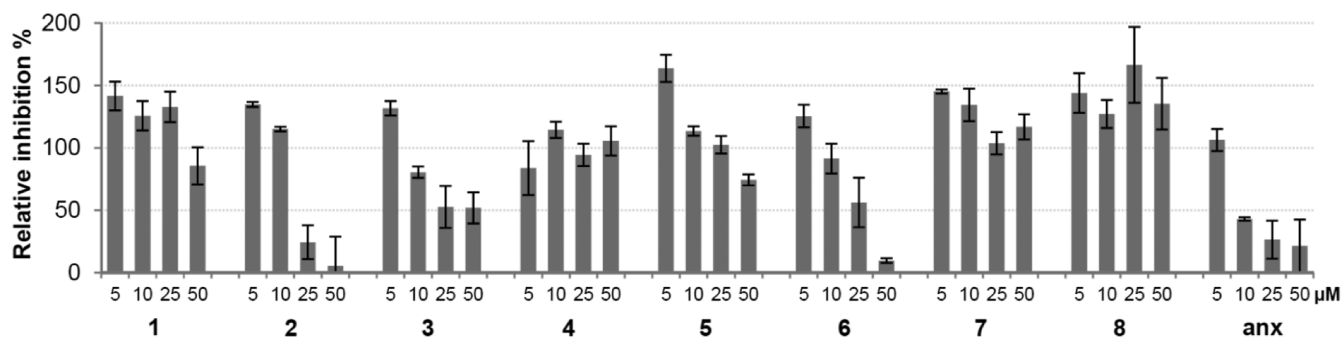


**Figure 6.** Effects of anginex and its  $\alpha/\beta$ -analogs on the proliferation of the bEND.3 mouse microvascular endothelial cell line. Cells were pretreated with or without the peptides for 1 h, and then, after washing, further cultured for 3 days. Proliferation was measured by using XTT test, and the values are given as percentages of the cell proliferation in the absence of peptides.

sequences with  $\alpha \rightarrow \beta^3$  mutations located distant from the hydrophobic core of the  $\beta$ -sheet (1 and 6). In line with the CD findings, the  $H\alpha$  chemical shifts of anginex displayed downfield shifts in response to increasing temperature<sup>58</sup> (Figure S7), indicating that the higher CD intensities at 217 nm reflected more stable  $\beta$ -sheets.<sup>4</sup> For 1 and 6, the  $H\alpha$  downfield shifts could be observed, but overall, the  $\alpha/\beta$ -derivatives exhibited decreased or missing temperature-dependent response.

These CD and NMR findings strongly suggested that the hydrophobic interactions are scaled down in the  $\alpha/\beta$ -analogs relative to anginex, and this supported that the structure-breaking effects of the  $\beta^3$ -residues were also exerted through disruption of the hydrophobic packing and self-association.

**Inhibition of Proliferation of Endothelial Cells.** The DPC-induced  $\beta$ -sheets of the  $\alpha/\beta$  analogs held promise for retained bioactivity. Anginex has been shown to exert *in vitro* antiproliferative effects in several vascular endothelial cell lines.<sup>39,41,47,59</sup> In our experiments, bEND.3, a mouse brain microvascular endothelial cell line previously shown to be more sensitive to anginex treatment than other murine cell lines,<sup>41</sup> was used to test the biological effects. Anginex displayed an IC<sub>50</sub> value of 21.8  $\mu$ M. The  $\alpha/\beta$  analogs 2, 3, and 6 displayed significant dose-dependent inhibition with IC<sub>50</sub> values of 29.8, 44.2, and 29.7  $\mu$ M, respectively (Figure 6). The antiproliferative activities of sequences 2 and 6 were comparable with that of the parent anginex. These results suggested that the inducible  $\beta$ -sheet was sufficient for the retention of this particular bioactivity. Analogs 1, 4, 5, 7, and 8 showed no significant inhibitory effect. We note that enhancements of the endothel proliferation at low concentrations compared to the control were observed for 5, 7, and 8, but this effect did not show concentration-dependence. Similar enhancements have been found for anginex-related sequences in the literature.<sup>47</sup> Key residues of anginex were previously identified in sequence-activity relationship studies, including Ala-scan.<sup>39,48</sup> Our substitution strategy affected some of these key residues: Val7 and Leu24 in 1, Val22 in 3, Leu11 and Ile20 in 5. The bioactivity of peptide 3 strongly supported that these side-chains were properly oriented in the  $\alpha/\beta$ -peptide analog. In contrast, peptide 1 did not display an antiproliferative effect in spite of its relatively high folding propensity. This could be explained by the substitution of two key residues in this peptide, which could result in a geometrically unfavorable side-chain presentation over the molecular surface and incompatibility with the pharmacophore pattern.

## CONCLUSIONS

Through a systematic  $\alpha \rightarrow \beta^3$  substitution approach, eight foldameric analogs of anginex were synthesized with  $\beta^3$ -amino acid building blocks in the  $\beta$ -sheet region. The mutated sequences display decreased folding propensities,<sup>35,36</sup> whereas an interacting partner (DPC) can induce  $\beta$ -sheet formation in a very similar way to that of the parent anginex. The reduction in  $\beta$ -sheet content is dependent on the position of the  $\beta^3$ -residues relative to the  $\beta$ -sheet core:  $\alpha \rightarrow \beta^3$  substitutions in the core region give rise to a greater destructuring effect than those at the edge. Analyses of the effects of the substitution patterns and the local geometry of the  $\beta^3$ -residues with branching next to the  $C\beta$  ( $\beta^3V$  and  $\beta^3I$ ) suggest that the destructuring effect is not primarily due to the potentially impaired H-bonding network around the  $\beta^3$  building blocks. The temperature-dependent measurements have revealed that the hydrophobic driving forces are scaled down in the  $\alpha/\beta$ -peptidic analogs. This can be explained by the backbone curvature and the angled side-chain of the  $\beta^3$ -residues relative to the best plane of the  $\beta$ -sheet, which are possibly not fully compatible with the packing requirements of the hydrophobic interactions. Structure–function analysis demonstrates that, inducibility of the appropriate secondary structure of the foldameric  $\alpha/\beta$ -peptidic anginex analogs is sufficient to diminish endothelial cell proliferation. Although  $\alpha \rightarrow \beta^3$  replacements can also be better tolerated than Ala mutations,<sup>60</sup> certain  $\alpha \rightarrow \beta^3$  substitutions may also affect the geometry of the side-chain display, which could break down the bioactivity. The design of an  $\alpha/\beta$ -peptidic  $\beta$ -sheet mimetic with the proposed approach can result in biologically useful materials. Moreover, the general tendency to uncontrolled aggregation of the  $\beta$ -sheet proteins can be tamed with this approach, and the insertion of the homologated residues improves the enzyme resistance and thereby the pharmacokinetic properties.

## EXPERIMENTAL SECTION

**Peptide Synthesis and Purification.** The synthesis of the sequences with microwave irradiation led to byproducts: aspartimide formation between D26-G27 and epimerization of D33. The byproducts were eliminated by using Fmoc-Asp(OtBu)-Gly(DMb)-OH (Novabiochem) for D26-G27 coupling. Tentagel R RAM resin was used as solid support and HATU as coupling reagent. Couplings were performed in a 3-equiv amino acid excess at 75 °C for 15 min for  $\alpha$ -amino acids, and for 30 min for  $\beta^3$ -residues. Histidine was coupled at 50 °C; arginines were coupled in two cycles. Peptides were cleaved with TFA/water/*D,L*-dithiothreitol/triisopropylsilane (90:5:2.5:2.5), then precipitated in ice-cold diethylether. The resin was washed with acetic acid and water, then filtered, and lyophilized. Peptides were

purified with RP-HPLC on a C18 column (Phenomenex Jupiter, 4.6 × 250 mm). HPLC eluents were the following: (A) 0.1% TFA in water and (B) 0.1% TFA, 80% ACN in water, with a gradient from 30% to 60% B in 60 min, at a flow rate of 4 mL min<sup>-1</sup>. Purity was confirmed by analytical RP-HPLC and ESI MS measurements.

**Circular Dichroism Measurements.** Circular dichroism measurements were performed with a Jasco J-815 CD-Spectrometer. CD spectra were recorded by using a 1 mm thermally jacketed quartz cuvette, from 260 to 190 nm, at a scan speed of 100 nm min<sup>-1</sup> with 8 accumulations. The peptide concentration was 100 μM in pH 5.6 K-phosphate buffer with or without 2.5 mM DPC. For thermal control, a Julabo water thermostat was used with a 10 min equilibration time for each temperature. Solvent baseline was subtracted.

**NMR Experiments.** NMR spectra were recorded on a Bruker Avance III 600 MHz spectrometer equipped with a 5 mm CP-TCI triple-resonance cryoprobe. Compounds were dissolved at a concentration of 0.5 mM in 20 mM, pH 5.6 d<sub>18</sub>-HEPES buffer (90% H<sub>2</sub>O, 10% D<sub>2</sub>O) containing 0.02% NaN<sub>3</sub>. For referencing, 4,4-dimethyl-4-silapentane-1-sulfonic acid (DSS) was used as an external standard. For resonance assignment, 2D homonuclear TOCSY and NOESY, and 2D heteronuclear <sup>15</sup>N and <sup>13</sup>C HSQC experiments were performed. The NOESY mixing time was 225 ms and the number of scans was 32. TOCSY measurements were made with homonuclear Hartman–Hahn transfer, using the DIPSI2 sequence for mixing, with a mixing time of 80 ms; the number of scans was 32. For all the 2D homonuclear spectra, 2K time domain points and 512 increments were applied. <sup>13</sup>C HSQC experiments were performed under the same sample conditions, but the buffer was prepared in D<sub>2</sub>O. Signal assignment was based on the 2D NMR spectra obtained at 37 °C. 1D <sup>1</sup>H NMR spectra of the 0.5 mM samples were also measured in pH 5.6 K-phosphate buffer at 37 °C, with or without 2.5 mM d<sub>18</sub>-DPC. All <sup>1</sup>H spectra were acquired with the excitation sculpting solvent suppression pulse scheme.<sup>61</sup> Processing was carried out by using Topspin 3.1 (Bruker), a cosine-bell window function, single-zero filling, and automatic baseline correction. Spectra were analyzed by Sparky 3.114 (T. D. Goddard and D. G. Kneller, University of California, San Francisco).

The secondary structure propensity (SSP)<sup>54</sup> score was calculated by using the ssp software. The refDB random coil reference set based on the chemical shifts of properly referenced known protein structures<sup>62</sup> was used.

**Pulsed Field-Gradient Spin Echo (PFGSE) NMR Measurements.** PFGSE NMR measurements were performed at 37 °C by using the stimulated echo and longitudinal eddy current delay (LED) pulse sequence with excitation sculpting for water suppression.<sup>63</sup> A time of 3 ms was used for the dephasing/refocusing gradient pulse length, and 300 ms for the diffusion delay. The gradient strength was changed quadratically (from 5% to 80% of the maximum value); the number of steps was 32. Each measurement was run with 64 scans and 8K time domain points. DOSY spectra were processed and evaluated by using the exponential fit implemented in Topspin 3.1. For processing, exponential window function and single zero filling were applied. The aggregation numbers were calculated from the Stokes–Einstein equation and trimethylsilyl propanoic acid (TSP) was utilized as an external volume standard.

**Endothelial Proliferation Assay.** Murine brain endothelial cell line bEND.3 was cultured in DMEM containing 10% fetal calf serum. The endothelial cells (900 cells/well) were plated onto a 96-well tissue culture plate and incubated for 1 h in the presence or absence of different concentrations (5, 10, 25, and 50 μM) of anginex or anginex analogs (dissolved in DMSO and diluted in 10 mM HEPES pH 7.4 containing 150 mM NaCl). The incubation time of 1 h was selected to eliminate uncontrolled peptide aggregation in the cell culture medium leading to nonspecific effects. Cells in control samples were treated with an equivalent amount of the solvent (DMSO and HEPES-NaCl). After incubation for 1 h, bEND.3 cells were washed twice with HEPES-NaCl, and then cultured further for 3 days. The proliferation of bEND.3 was measured by XTT assay<sup>64</sup> according to the manufacturer's instruction (Sigma-Aldrich). For the last 2 h, XTT was added to the samples and the resulting absorbance was measured

with a Microplate Reader (Multiskan, Thermo Electron Corporation) at 450 nm. The experiments were repeated three times in triplicate.

## ■ ASSOCIATED CONTENT

### § Supporting Information

Detailed NMR and CD data in Supporting Figures S1–S7 and in Supporting Tables 1 and 2; peptide characterization data; modeling details. This material is available free of charge via the Internet at <http://pubs.acs.org>.

## ■ AUTHOR INFORMATION

### Corresponding Author

[martinek@pharm.u-szeged.hu](mailto:martinek@pharm.u-szeged.hu)

### Author Contributions

<sup>§</sup>Z.H. and E.W. contributed equally.

### Notes

The authors declare no competing financial interest.

## ■ ACKNOWLEDGMENTS

This work was supported by the Hungarian Research Foundation (OTKA K83882), and the Hungarian Academy of Sciences, Lendület program (LP-2011-009). Csaba Vizler is gratefully acknowledged for providing the bEND.3 cell line.

## ■ REFERENCES

- (1) Guerois, R.; López de la Paz, M. *Protein Design: Methods and Applications*; Humana Press: Totowa, N.J., 2006.
- (2) Gellman, S. H. *Curr. Opin. Chem. Biol.* **1998**, *2*, 717.
- (3) Ramírez-Alvarado, M.; Kortemme, T.; Blanco, F. J.; Serrano, L. *Bioorg. Med. Chem.* **1999**, *7*, 93.
- (4) Mayo, K. H.; Ilyina, E.; Park, H. *Protein Sci.* **1996**, *5*, 1301.
- (5) Searle, M. S. *Pept. Sci.* **2004**, *76*, 185.
- (6) Espinosa, J. F.; Syud, F. A.; Gellman, S. H. *Protein Sci.* **2002**, *11*, 1492.
- (7) Stanger, H. E.; Gellman, S. H. *J. Am. Chem. Soc.* **1998**, *120*, 4236.
- (8) Ramírez-Alvarado, M.; Blanco, F. J.; Serrano, L. *Nat. Struct. Mol. Biol.* **1996**, *3*, 604.
- (9) Alba, E. d.; Jiménez, M. A.; Rico, M.; Nieto, J. L. *Folding Des.* **1996**, *1*, 133.
- (10) Mayo, K. H.; Haseman, J.; Ilyina, E.; Gray, B. *Biochim. Biophys. Acta* **1998**, *142S*, 81.
- (11) Fernandez-Escamilla, A. M.; Ventura, S.; Serrano, L.; Jimenez, M. A. *Protein Sci.* **2006**, *15*, 2278.
- (12) Kortemme, T.; Ramírez-Alvarado, M.; Serrano, L. *Science* **1998**, *281*, 253.
- (13) Syud, F. A.; Stanger, H. E.; Mortell, H. S.; Espinosa, J. F.; Fisk, J. D.; Fry, C. G.; Gellman, S. H. *J. Mol. Biol.* **2003**, *326*, 553.
- (14) Alba, E. D.; Santoro, J.; Rico, M.; Jiménez, M. A. *Protein Sci.* **1999**, *8*, 854.
- (15) Schenck, H. L.; Gellman, S. H. *J. Am. Chem. Soc.* **1998**, *120*, 4869.
- (16) Sharman, G. J.; Searle, M. S. *J. Am. Chem. Soc.* **1998**, *120*, 5291.
- (17) Lim, A.; Makhov, A. M.; Saderholm, M. J.; Griffith, J. D.; Erickson, B. W. *Biochem. Biophys. Res. Commun.* **1999**, *264*, 498.
- (18) Lim, A.; Saderholm, M. J.; Makhov, A. M.; Kroll, M.; Yan, Y.; Perera, L.; Griffith, J. D.; Erickson, B. W. *Protein Sci.* **1998**, *7*, 1545.
- (19) Yan, Y.; Erickson, B. W. *Protein Sci.* **1994**, *3*, 1069.
- (20) Robinson, J. A. *Acc. Chem. Res.* **2008**, *41*, 1278.
- (21) Chung, Y. J.; Huck, B. R.; Christianson, L. A.; Stanger, H. E.; Krauthauser, S.; Powell, D. R.; Gellman, S. H. *J. Am. Chem. Soc.* **2000**, *122*, 3995.
- (22) Chung, Y. J.; Huck, B. R.; Christianson, L. A.; Stanger, H. E.; Krauthauser, S.; Powell, D. R.; Gellman, S. H. *J. Am. Chem. Soc.* **2001**, *123*, 5851.
- (23) Seebach, D.; Abele, S.; Gademann, K.; Jaun, B. *Angew. Chem., Int. Ed.* **1999**, *38*, 1595.

- (24) Jones, C. R.; Qureshi, M. K. N.; Truscott, F. R.; Hsu, S. T. D.; Morrison, A. J.; Smith, M. D. *Angew. Chem., Int. Ed.* **2008**, *47*, 7099.
- (25) Khurram, M.; Qureshi, N.; Smith, M. D. *Chem. Commun.* **2006**, 5006.
- (26) Vass, E.; Strijowski, U.; Wollschläger, K.; Mándity, I. M.; Szilvágyi, G.; Jewgiński, M.; Gaus, K.; Royo, S.; Majer, Z.; Sewald, N.; Hollósi, M. *J. Pept. Sci.* **2010**, *16*, 613.
- (27) Nowick, J. S. *Acc. Chem. Res.* **2008**, *41*, 1319.
- (28) Cheng, P. N.; Liu, C.; Zhao, M.; Eisenberg, D.; Nowick, J. S. *Nat. Chem.* **2012**, *4*, 927.
- (29) Segman, S.; Lee, M. R.; Vaiser, V.; Gellman, S. H.; Rapaport, H. *Angew. Chem., Int. Ed.* **2010**, *49*, 716.
- (30) Martinek, T. A.; Hetenyi, A.; Fulop, L.; Mandity, I. M.; Toth, G. K.; Dekany, I.; Fulop, F. *Angew. Chem., Int. Ed.* **2006**, *45*, 2396.
- (31) Chandrasekhar, S.; Babu, B. N.; Prabhakar, A.; Sudhakar, A.; Reddy, M. S.; Kiran, M. U.; Jagadeesh, B. *Chem. Commun. (Cambridge, U.K.)* **2006**, 1548.
- (32) Torres, E.; Gorrea, E.; Burusco, K. K.; Da Silva, E.; Nolis, P.; Rua, F.; Boussert, S.; Diez-Perez, I.; Dannenberg, S.; Izquierdo, S.; Giralt, E.; Jaime, C.; Branchadell, V.; Ortuno, R. M. *Org. Biomol. Chem.* **2010**, *8*, 564.
- (33) Rua, F.; Boussert, S.; Parella, T.; Diez-Perez, I.; Branchadell, V.; Giralt, E.; Ortuno, R. M. *Org. Lett.* **2007**, *9*, 3643.
- (34) Chandrasekhar, S.; Sudhakar, A.; Kiran, M. U.; Babu, B. N.; Jagadeesh, B. *Tetrahedron Lett.* **2008**, *49*, 7368.
- (35) Lengyel, G. A.; Frank, R. C.; Horne, W. S. *J. Am. Chem. Soc.* **2011**, *133*, 4246.
- (36) Lengyel, G. A.; Horne, W. S. *J. Am. Chem. Soc.* **2012**, *134*, 15906.
- (37) Sonti, R.; Gopi, H. N.; Muddegowda, U.; Ragothama, S.; Balaran, P. *Chemistry* **2013**, *19*, 5955.
- (38) Horne, W. S.; Gellman, S. H. *Acc. Chem. Res.* **2008**, *41*, 1399.
- (39) Griffioen, A. W.; van der Schaft, D. W.; Barendsz-Janson, A. F.; Cox, A.; Struijker Boudier, H. A.; Hillen, H. F.; Mayo, K. H. *Biochem. J.* **2001**, *354*, 233.
- (40) Dings, R. P.; van der Schaft, D. W.; Hargittai, B.; Haseman, J.; Griffioen, A. W.; Mayo, K. H. *Cancer Lett.* **2003**, *194*, 55.
- (41) van der Schaft, D. W.; Dings, R. P.; de Lussanet, Q. G.; van Eijk, L. I.; Nap, A. W.; Beets-Tan, R. G.; Bouma-Ter Steege, J. C.; Wagstaff, J.; Mayo, K. H.; Griffioen, A. W. *FASEB J.* **2002**, *16*, 1991.
- (42) Wang, J. B.; Wang, M. D.; Li, E.; Dong, D. F. *Peptides* **2012**, *38*, 457.
- (43) Thijssen, V. L.; Postel, R.; Brandwijk, R. J.; Dings, R. P.; Nesmelova, I.; Satijn, S.; Verhofstad, N.; Nakabeppu, Y.; Baum, L. G.; Bakkers, J.; Mayo, K. H.; Poirier, F.; Griffioen, A. W. *Proc. Natl. Acad. Sci. U. S. A.* **2006**, *103*, 15975.
- (44) Mayo, K. H.; Ilyina, E. *Protein Sci.* **1998**, *7*, 358.
- (45) Arroyo, M. M.; Mayo, K. H. *Biochim. Biophys. Acta* **2007**, *1774*, 645.
- (46) Dings, R. P.; Arroyo, M. M.; Lockwood, N. A.; van Eijk, L. I.; Haseman, J. R.; Griffioen, A. W.; Mayo, K. H. *Biochem. J.* **2003**, *373*, 281.
- (47) Mayo, K. H.; van der Schaft, D. W.; Griffioen, A. W. *Angiogenesis* **2001**, *4*, 45.
- (48) Mayo, K. H.; Dings, R. P. M.; Flader, C.; Nesmelova, I.; Hargittai, B.; van der Schaft, D. W. J.; van Eijk, L. I.; Walek, D.; Haseman, J.; Hoyer, T. R.; Griffioen, A. W. *J. Biol. Chem.* **2003**, *278*, 45746.
- (49) Stafford, R. E.; Fanni, T.; Dennis, E. A. *Biochemistry* **1989**, *28*, 5113.
- (50) Liu, D. Z.; LeCluyse, E. L.; Thakker, D. R. *J. Pharm. Sci.* **1999**, *88*, 1161.
- (51) Manzo, G.; Carboni, M.; Rinaldi, A. C.; Casu, M.; Scorciapino, M. A. *Magn. Reson. Chem.* **2013**, *51*, 176.
- (52) Wishart, D. S.; Sykes, B. D.; Richards, F. M. *Biochemistry* **1992**, *31*, 1647.
- (53) Wishart, D. S.; Nip, A. M. *Biochem. Cell Biol.* **1998**, *76*, 153.
- (54) Marsh, J. A.; Singh, V. K.; Jia, Z.; Forman-Kay, J. D. *Protein Sci.* **2006**, *15*, 2795.
- (55) Raguse, T. L.; Lai, J. R.; Gellman, S. H. *Helv. Chim. Acta* **2002**, *85*, 4154.
- (56) Wilkins, D. K.; Grimshaw, S. B.; Receveur, V.; Dobson, C. M.; Jones, J. A.; Smith, L. J. *Biochemistry* **1999**, *38*, 16424.
- (57) Chandler, D. *Nature* **2005**, *437*, 640.
- (58) Fesinmeyer, R. M.; Hudson, F. M.; Olsen, K.; White, G. N.; Euser, A.; Andersen, N. J. *Biomol. NMR* **2005**, *33*, 213.
- (59) Brandwijk, R. J.; Dings, R. P.; van der Linden, E.; Mayo, K. H.; Thijssen, V. L.; Griffioen, A. W. *Biochem. Biophys. Res. Commun.* **2006**, *349*, 1073.
- (60) Haase, H. S.; Peterson-Kaufman, K. J.; Lan Levensgood, S. K.; Checco, J. W.; Murphy, W. L.; Gellman, S. H. *J. Am. Chem. Soc.* **2012**, *134*, 7652.
- (61) Hwang, T. L.; Shaka, A. J. *J. Magn. Reson., Ser. A* **1995**, *112*, 275.
- (62) Zhang, H.; Neal, S.; Wishart, D. S. *J. Biomol. NMR* **2003**, *25*, 173.
- (63) Balayssac, S.; Delsuc, M. A.; Gilard, V.; Prigent, Y.; Malet-Martino, M. *J. Magn. Reson.* **2009**, *196*, 78.
- (64) Berridge, M. V.; Herst, P. M.; Tan, A. S. *Biotechnol. Annu. Rev.* **2005**, *11*, 127.